Available online at www.sciencedirect.com

ScienceDirect

Procedia Computer Science 207 (2022) 726–735

Procedia Computer Science

www.elsevier.com/locate/procedia

26th International Conference on Knowledge-Based and Intelligent Information & Engineering Systems (KES 2022)

Fully automatic segmentation of the choroid in non-EDI OCT images of patients with multiple sclerosis

Emilio López-Varela[a,b,*], Noelia Barreira[a,b], Nuria Olivier Pascual[c], Emma Garcia Ben[c], Sara Rubio Cid[c], Manuel G. Penedo[a,b]

[a] *VARPA Group, Biomedical Research Institute of A Coruña (INIBIC), University of A Coruña, Xubias de Arriba 84, A Coruña 15006, Spain*
[b] *CITIC-Research Center of Information and Communication Technologies, University of A Coruña, Campus de Elviña s/n, A Coruña 15071, Spain*
[c] *Servizo de Oftalmoloxía, Complejo Hospitalario Universitario de Ferrol (CHUF), Av. da Residencia S/N, Ferrol 15405, Spain*

Abstract

Multiple Sclerosis (MS) is a chronic neurological disease, in which immune-mediated mechanisms lead to pathological processes of neurodegeneration. Optical coherence tomography (OCT) has recently begun to be used to diagnose and monitor patients with MS. Morphological changes in the choroid have been linked to the onset of MS, so an accurate segmentation of this layer is critical. Conventional OCT has several limitations in obtaining accurate images of the choroid, which has been improved through the use of systems such as Enhanced Depth Imaging (EDI) OCT. Unfortunately, many longitudinal studies that have collected samples over the years in the past have been performed using highly variable settings and without the use of the EDI protocol (or similar variants). For these reasons, in this work we propose a series of fully automatic approaches, based on convolutional neural networks, capable of robustly segmenting the choroid in OCT images without using the EDI protocol. To test the robustness and efficiency of our method, we performed experiments on a public dataset and a collected one. The Dice score obtained by the best proposed architecture is 89.7 for the public dataset, and 93.7 for the collected dataset.

© 2022 The Authors. Published by Elsevier B.V.
This is an open access article under the CC BY-NC-ND license (https://creativecommons.org/licenses/by-nc-nd/4.0)
Peer-review under responsibility of the scientific committee of the 26th International Conference on Knowledge-Based and Intelligent Information & Engineering Systems (KES 2022)

Keywords: Optical Coherence Tomography; Multiple Sclerosis; Choroid segmentation; Convolutional Neural Networks

1. Introduction

Multiple Sclerosis (MS) is a chronic neurological disease of the central nervous system, in which immune-mediated mechanisms lead to pathological processes of inflammation and neurodegeneration [18]. MS mainly affects young adults, and is currently the leading cause of non-traumatic neurological disability in this population group. Approximately 50% of affected patients will require walking assistance within 15 years of disease onset, and 2/3 of them

* Corresponding author. Tel.: +34-881011330; fax: +34-981167160.
E-mail address: e.lopezv@udc.es

1877-0509 © 2022 The Authors. Published by Elsevier B.V.
This is an open access article under the CC BY-NC-ND license (https://creativecommons.org/licenses/by-nc-nd/4.0)
Peer-review under responsibility of the scientific committee of the 26th International Conference on Knowledge-Based and Intelligent Information & Engineering Systems (KES 2022)
10.1016/j.procs.2022.09.128

will be unable to carry out their usual work activities. This has a serious impact on the economic burden of patients, impairing their quality of life and limiting their personal relationships [23]. According to the results of the Global Burden Disease Study 2016 [26], the average prevalence of MS is increasing since the 1990s, being currently about 30 cases per 100,000 population. This increase in prevalence, coupled with the deterioration in the quality of life of patients suffering from this disease, motivate the creation of new treatments and techniques for early detection and monitoring of the disease.

One of the main techniques used for the detection and follow-up of MS is magnetic resonance imaging (MRI). However, like any diagnostic test, MRI has limitations. An abnormal MRI does not necessarily imply the existence of MS, as there are other diseases that cause very similar brain damage. On the other hand, an MRI with a normal result does not completely rule out MS, as there may be spinal cord damage or lesions not visible on the MRI. Finally, the use of MRI is limited by other factors such as its cost and the long time needed to obtain the images [10]. These reasons led to the use of alternative imaging techniques to characterize and detect MS, such as Optical Coherence Tomography (OCT). OCT is a non-invasive in vivo technique based on the different reflectance of the layers present in the ocular structure that allows the acquisition of cross-sectional images of the retina with semi-histological resolution. The OCT volumes can be obtained in different regions of the eye (macular, peripapillary, etc.) using different configuration parameters. This results in volumes with different resolutions, number of slices and characteristics depending on the region and way of capture [17, 16].

Several clinical studies have linked changes in different retinal layers to the development of MS [2, 6, 5, 8, 7] so OCT has recently started to be used to detect and characterize MS. One of the relevant biomarkers for the analysis of MS on OCT images is the characterization of changes in the choroid, a vascular tissue that provides oxygen and nutrition to the outer retinal layers. Different morphological changes in the choroid have been related to the onset and progression of MS, so accurate segmentation of this layer is essential to diagnose and follow the progression of MS using OCT imaging. In contrast to the other retinal layers, the choroid is usually segmented manually in the clinical setting which is time consuming and laborious. So a fully automated system is significantly useful, helping clinicians to make a decision about diagnosis and treatments more robustly, reducing the subjectivity of the process. However, conventional OCT has several limitations in obtaining accurate images of the choroid. The choroid is located posterior to the retinal pigment epithelium (RPE), a layer that absorbs large amounts of light. This, together with the light scattering caused by the dense vascular structure of the choroid, results in a poorly defined choroid in conventional OCT images, limiting and hindering its characterization and segmentation due to its diffuse structure and boundaries [28]. To solve these problems and improve the visualization of the choroid, in 2008, Spaide *et al.* proposed the EDI-OCT (Enhanced Depth Imaging OCT) system. [24]. Essentially, in this system the spectral domain OCT objective lens is placed closer to the eye. This causes the backscattered light from the choroid to be closer to the zero-delay line producing an image where the choroid is much more sharply defined. In Figure 1 an image obtained using the EDI protocol and three images obtained using a conventional OCT are shown. The difference between the two types can be seen at the lower limit of the choroid. Unfortunately, many longitudinal studies that have collected samples over the years in the past as well as current clinical analyses have been performed without the use of the EDI protocol (or similar variants). Moreover, these studies have been performed in different regions of the eye, using OCT capture devices with different configurations, resulting in studies with quite diverse OCT images. For all these reasons, there is a need for a fully automatic system capable of robustly segmenting the choroid in images obtained in different regions of the eye without using the EDI protocol.

Due to the great relevance of general layer segmentation for different pathologies, several works have been proposed aiming at choroid segmentation [12, 29, 22]. Salafian *et al*. [22] presented an automatic choroidal segmentation method based on transforming each EDI-OCT image to a neutrosophic space. On the other hand, in Kajic *et al*. [12], a two-stage texture-based statistical model for choroidal segmentation of normal and pathological eyes was presented. Recently, convolutional neural networks have been applied to segment images obtained from various imaging modalities vastly improving the results obtained with classical methods [27, 1, 19]. Regarding the segmentation of different retinal layers, the most commonly used models are encoder-decoder variants of fully convolutional network architectures [15] such as the UNet [21]. In George *et al*. [9], a Chan Vese model for segmenting EDI-OCT images of cornea and choroid in the macula region was presented. In Chen *et al*. [3], the choroid is segmented in macular EDI-OCT images using a convolutional neural network that detects the lower and upper edges of the choroid. Finally, in Li *et al*. [13], all retinal layers are segmented in peripapillary images of glaucoma patients using a two-stage multiscale

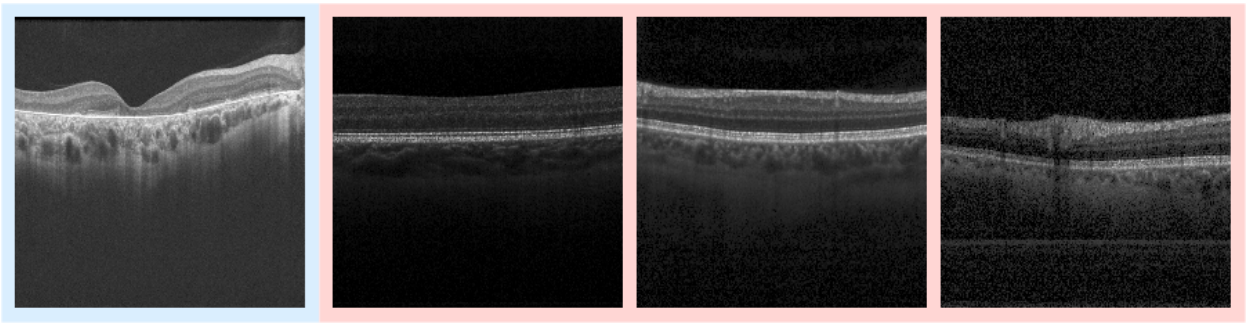

Fig. 1. Image obtained using the EDI protocol (left) and three images obtained using conventional OCT (right).

convolutional neural network. In summary, all of the state of the art works presented here propose methods to segment the choroid, or alternatively find the upper and lower boundaries, in an accurate manner in different pathologic contexts. All of these papers use images of a single region (either macular or peripapillary) or use EDI or similar enhanced images captured with a single configuration. As previously discussed, the problem is that many routine clinical studies as well as longitudinal studies collected in the past have been created without using the EDI protocol. In addition, the use of OCT images obtained in a single region of the eye (either macular or peripapillary) with a specific parameter setting is limited in their potential clinical utility. All these factors make it important to develop a segmentation method capable of robustly segmenting the choroid in OCT images obtained in different regions of the eye using different settings and without using EDI.

In this work, we propose a robust approach, based on convolutional neural networks, for the automatic segmentation of the choroid in OCT non-EDI images with various configurations. In a series of experiments, we compare different neural architectures with various combinations of encoders to determine the best segmentation approach. To test both the robustness and the efficiency of our method, we performed experiments in two different datasets. Thus, we use a public dataset to compare our approaches with the state of the art and a collected dataset of non-EDI images captured with several settings in different eye regions from healthy and MS patients. To the best of our knowledge, this work is the first approach to attempt to segment the choroid in a large set of non-EDI OCT images with varying configurations.

2. Materials and Methods

2.1. Datasets

Two different datasets were used to carry out the experiments. We used the public dataset collected by Li *et al* for comparison with the state of the art [13]. This dataset consists of peripapillary OCT images obtained from 61 subjects using the DRI OCT-1 Atlantis (Topcon Corporation, Tokyo, Japan). Each image is labeled with several retinal layers including the choroid. In our case we used only the choroid label to perform our experiments. More details about this dataset can be found at [13].

Additionally, we collect a dataset that consists of a total of 224 images with different configurations, randomly extracted from 50 OCT cubes from a previous study. These cubes belong to 37 different subjects where 22 of the 37 subjects and, respectively, 103 of the 224 images correspond to healthy subjects while 15 subjects and 121 images correspond to patients suffering from MS. All cubes were created using two equivalent Spectralis R OCT capture devices from Heidelberg Engineering. Within these cubes there are four different types of cubes in which both the eye region and the resolution of the images vary. The first type corresponds to radial OCT cubes with 27 slices centered in the peripapillary region, whereas the remaining three types correspond to cubes centered in the macular region. The second type corresponds to cubes with 61 slices of the posterior pole and an image resolution of 768 x 496. The third type corresponds to cubes with 25 slices centered on the macula and an image resolution of 512 x 496. Finally, the fourth type corresponds to 512-slice cubes that are obtained as an intermediate by-product of an ophthalmological test frequently performed in the clinical setting and have a resolution of 512 x 496.

This set was divided into two groups. On the one hand, a group consisting of 196 images was used to train and test the models. The images in this group were labeled by an expert, so that each image has an associated segmentation mask, where all pixels were labeled as background or choroid. On the other hand, the remaining 28 images were labeled by three different medical experts. Each expert labeled the lower contour of the choroid in each image twice (once using the raw image and once using an image with improved local contrast) giving a total of six edge labels per image. This set of 28 images serves to validate whether there are differences between the segmentation performed by our approaches and that performed by different medical experts. Examples of both labelings can be seen in Figure 2.

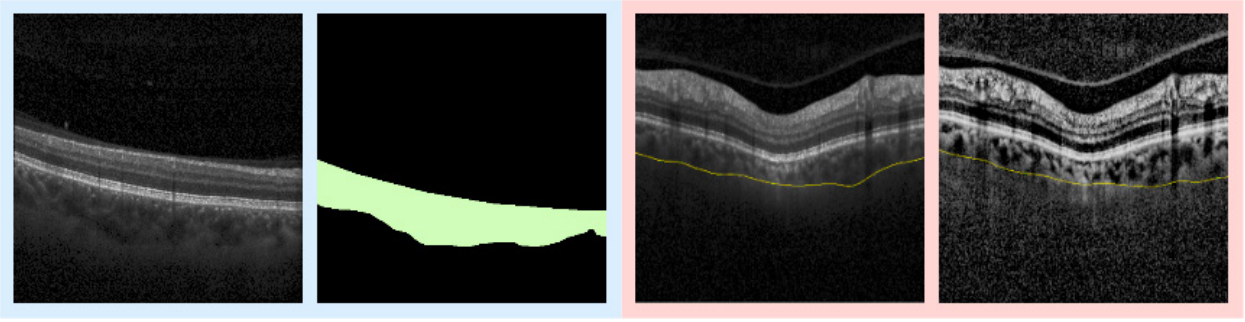

Fig. 2. On the left, an example of OCT image and its associated segmentation mask. On the right, an example of the contour line labeled by one of the experts in an example image.

2.2. Software and Hardware resources

This work was developed in Python (version 3.9.5) and using PyTorch (version 1.9.1 with cuda 11.2) [20] to create, train and validate the models. The encoders of the models were obtained from the PyTorch segmentation model library [30]. OpenCV (4.5.3) and Numpy (1.20.3) were used to perform image processing operations. Regarding Hardware, training and validation were carried out using an Intel(R) Core(TM) i9-9900K CPU @ 3.60GHz and an NVIDIA GeForce RTX 2080 Ti.

2.3. Network architectures

In this work, we study the application of several base architectures of convolutional neural networks to segment the choroid. As base architectures we use, on the one hand, the UNet [21], an architecture that extracts feature maps at different scales in a progressive manner. In this architecture, the loss of information is avoided through the use of skip connections, with which the feature maps are reconstructed at the original image size. On the other hand, we use a Feature Pyramid Network (FPN) [14] adapted to a semantic segmentation task. This type of architecture allows extracting feature maps at different scales, which are used together to perform the final model prediction. The feature maps obtained at different scales allow to make a more accurate segmentation of the different objects and their boundaries. Figure 3 shows the general structure of the UNet architecture (left) and the general structure of the FPN architecture (right). Each convolutional layer is followed by a batch normalization layer and a nonlinear layer. A Log Softmax is applied after the final convolutional layer in the channel axis. This way, the class of each pixel (background or choroid) is set by simply selecting the channel with the maximum value. The parts of each architecture that correspond to the network encoder, in charge of extracting and encoding the feature maps that will lead to the prediction, are represented in blue. It is essential to have a suitable encoder, which has the ability to extract feature maps containing all the necessary information to segment the target into images with many variations with different textures and noises. For this reason, for each of the architectures, we tested three different encoder configurations with different characteristics and number of parameters, resulting in six configurations. These encoders are part of neural architectures commonly used in similar application domains:

- Densely Connected Convolutional Network [11]: DenseNet networks are based on the progressive concatenation of features from previous layers in order to strengthen feature propagation. In this work the DenseNet201 was used as an encoder.
- Efficientnet [25]: Efficientnet corresponds to a family of models created by balancing network depth, width and resolution in an efficient and effective way. In this work, Efficientnet-bo and Efficientnet-b7 were used as encoders.

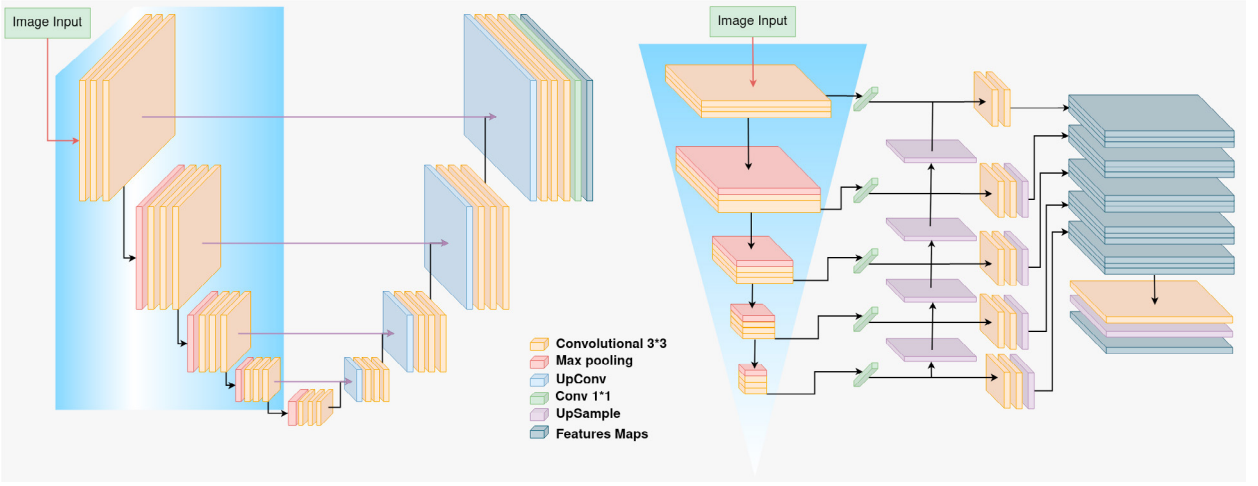

Fig. 3. General structure of the UNet architecture (left) and general structure of the FPN architecture (right). The parts of each architecture that correspond to the network encoder are represented in blue.

2.4. Training details

Regarding the public dataset, the parameters and the division of the dataset specified in the original work [13] were used. Specifically, the split ratio between the training, validation and test sets was 6:2:2. The learning rate was set to 0.001 and decreased by an order of magnitude every 20 epochs. Moreover, the Adam optimizer was used. We also divided the 196 images of the collected dataset into three parts, 100 images for training, 48 images for validation and 48 images for test. In each set the ratio of healthy and MS images was 54:46 and there was the same proportion of each OCT image type.

Regarding the training process, knowing the small size of our dataset and to avoid overfitting, the encoders of the models were first initialized using a pre-training on the ImageNet dataset [4]. The models were then pre-trained on the original public dataset. This greatly helps to adapt to our segmentation task by avoiding overfitting. Each of the models was trained on our dataset for 80 epochs, using an initial learning rate of 0.001 that was reduced by half an order of magnitude every 10 epochs. Momentum and weight decay coefficients were set to 0.9 and 0.0001 respectively. We used Adam as an optimizer to train the model with a batch size of 1. To make the model more robust and avoid overfitting, an exhaustive data augmentation process has also been applied. Some transformations were grouped so that only one from the group could be applied at a time. Table 1 shows all the transformations applied to the images. As loss function we use the sum of two loss functions. We use the Dice loss and the CrossEntropy loss (Eq. 1) where g_i and p_i indicates the ground truth and the probability in prediction of pixel x belonging to of class i, and M is the number of classes in the segmentation network.

$$Dice = 1 - \frac{1}{M}\sum_{i=1}^{M}\left(\frac{2\sum_{x\in\Omega} p_i(x)\cdot g_i(x)}{\sum_{x\in\Omega} p_i(x) + \sum_{x\in\Omega} g_i(x)}\right) \qquad CrossEntropy = -\frac{1}{M}\sum_{i=1}^{M} g_i\, log(p_i) \tag{1}$$

Table 1. Transformations applied to images in each batch. From each group only one transformation can be applied at a time.

	Group 1	Group 2	Group 3	Group 4	Group 5	Group 6	Group 7
Applied Transformations	Coarse Dropout	Elastic Transform, Piecewise Affine	Shift Scale Rotate	Horizontal Flip	Gaussian Blur, Blur	Brightness Contrast, CLAHE	Multiplicative Noise, Gauss Noise

Regarding model evaluation, all models were evaluated in two ways. On the one hand, for the test set of images, the Dice score (DSC) and pixel accuracy (PA) (Eq. 2) were obtained, where X represents the prediction region and Y is the ground truth region. On the other hand, for the 28 independent images where the lower contour was labeled, the Euclidean distance (EUC) (Eq. 2) was calculated. The values obtained by the network were compared with those obtained by the three medical experts using a student's t-test.

$$DSC = \frac{2 \cdot |X \cap Y|}{|X| + |Y|} \qquad PA = \frac{|X \cap Y|}{|Y|} \qquad EUC = \sqrt{(x_1 - x_2)^2 + (y_1 - y_2)^2} \tag{2}$$

3. Results and Discussion

3.1. Public dataset results

First, we show the results obtained by evaluating our models on the public dataset along with the state of the art. Table 2 shows the DSC and PA obtained for the different architectures tested along with the baseline of the dataset. Figure 4 shows an example of an OCT image with the overlay mask predicted by each network. These images show qualitatively the differences between the segmentations performed by the different networks as well as their errors. As can be seen, several models outperform the state of the art in choroid detection. Specifically, the FPN architecture using a Densenet201 as an encoder is particularly effective in this task.

Table 2. DSC and PA obtained for the segmentation of the public dataset for all the models tested. The best values are marked in bold.

Metric	Li *et al* [13]	UNet			FPN		
		Densenet 201	Efficient b0	Efficient b7	Densenet 201	Efficient b0	Efficient b7
DSC	89.2	89.5	88.8	89.3	**89.7**	88.9	89.4
PA	89.2	89.0	86.8	89.8	**90.0**	89.0	89.4

3.2. Collected dataset results

We compared the lower choroidal boundary detected by the networks with the average of the six labelings of the lower choroidal contour performed by the experts. The distances obtained for the three models using the UNet base architecture are 704 for Densenet201, 930 for Efficientnet-b0 and 695 for Efficientnet-b7. The distances obtained for the three models using the FPN base architecture are 657 for Densenet201, 881 for Efficientnet-b0 and 701 for Efficientnet-b7. For reference, the expert who performed the closest labeling to the mean of experts obtained a distance of 662. These results show that there are significant differences in the contours predicted by the different networks. Specifically UNet and FPN using Efficientnet-b0 as encoder give worse results than the other models. The results obtained by the best performing network (FPN Densenet) versus the six labelings performed by the experts are shown and compared in Figure 5. Table 3 shows an expert vs. expert confusion matrix (the network is also included), where the mean EUC obtained by comparing the contours labeled by one expert with each of the others is shown.

Table 4 shows the DSC and PA obtained for the different architectures tested. As can be seen, as in the case of the public dataset, the FPN using the Densenet201 is the network with the best segmentation results. Figure 6 shows several examples of segmentation masks obtained by this model. It can be seen how the network is able to segment

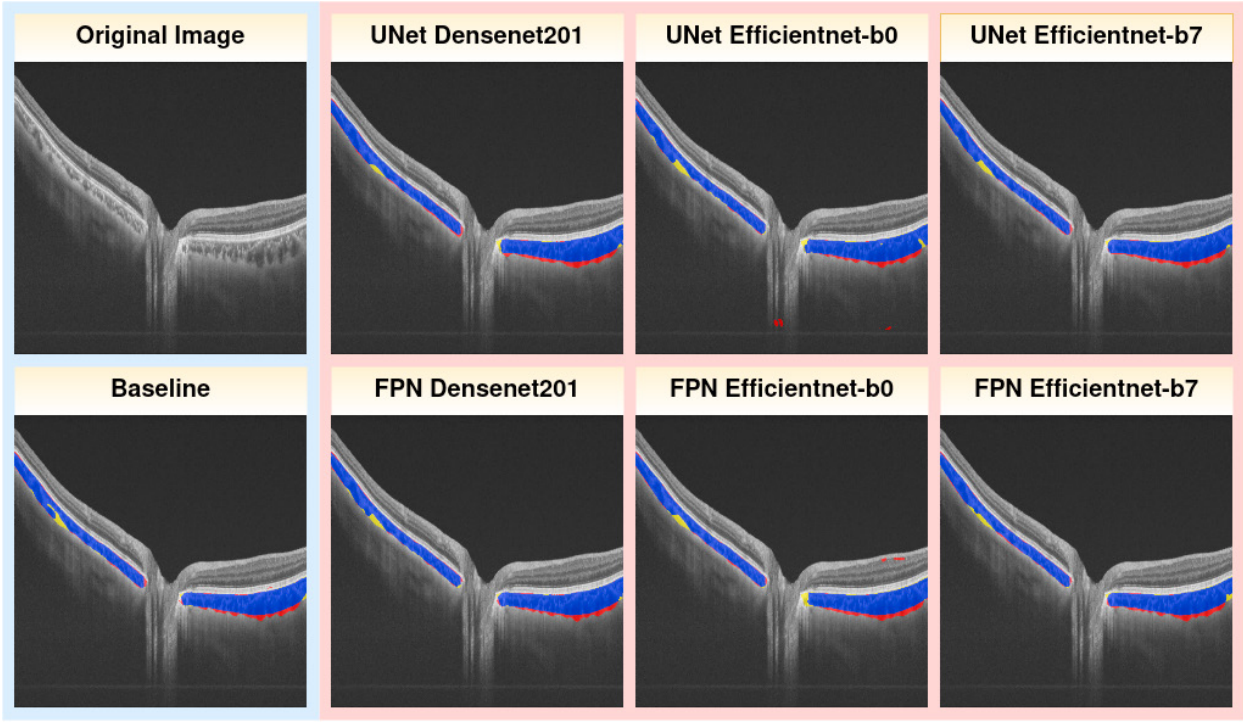

Fig. 4. Example of the segmentation masks predicted by the different models. Blue areas show the prediction that match the labeling, while red and yellow areas show the false positives and false negatives, respectively.

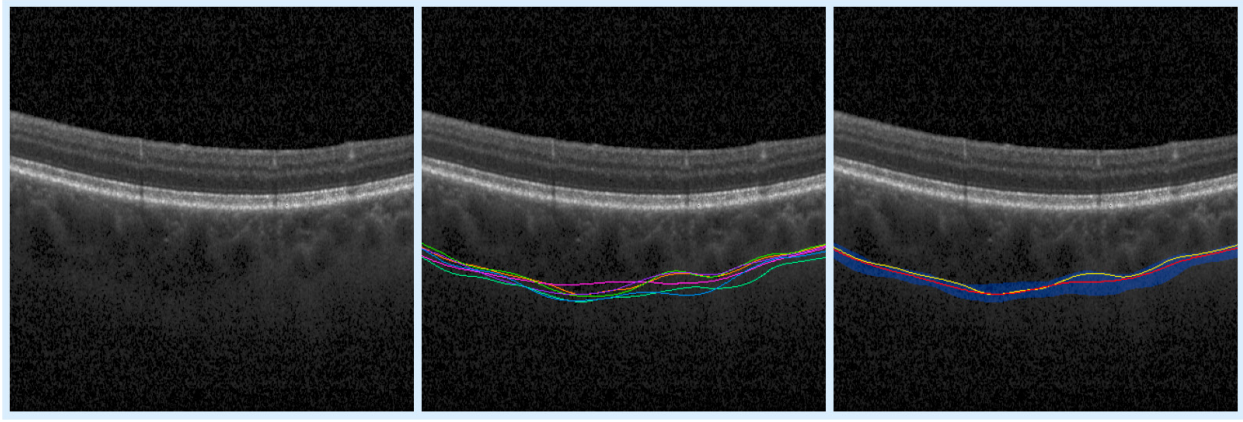

Fig. 5. From left to right: The original image, the contours delimited by the experts as well as the differences between the contours delimited by the network and the experts. In this last image, the contour delimited by the network is shown in yellow, the average contour is represented in red whereas the area of the dispersion of the contour is shown in blue.

the choroid in images with very different characteristics, even in images where the lower boundary of the choroid is subtle.

3.3. Discussion

The results presented show how several of the proposed approaches surpass the state of the art in segmenting the choroid, even without using the EDI protocol. Among the proposed approaches, the FPN using the Densenet201 encoder obtains the best segmentation results. As can be seen in Figure 5, there is some variability among medical

Table 3. Expert vs. expert confusion matrix, showing the mean EUC obtained by comparing the contours labeled by one expert with each of the others.

	Expert 1_1	Expert 1_2	Expert 2_1	Expert 2_2	Expert 3_1	Expert 3_2	Network
Expert 1_1	0	391	811	823	858	834	629
Expert 1_2	-	0	823	789	833	730	574
Expert 2_1	-	-	0	855	1130	976	832
Expert 2_2	-	-	-	0	985	951	783
Expert 3_1	-	-	-	-	0	867	807
Expert 3_2	-	-	-	-	-	0	711
Network	-	-	-	-	-	-	0

Table 4. DSC and PA obtained for the segmentation of the collected dataset by all the models tested. The best values are marked in bold.

Metric	UNet			FPN		
	Densenet 201	Efficient b0	Efficient b7	Densenet 201	Efficient b0	Efficient b7
DSC	92.5	89.0	93.0	**93.7**	91.6	93.1
PA	90.5	88.8	91.1	**92.3**	88.2	90.1

experts when it comes to delimiting the lower contour of the choroid. This is due to the fact that this contour is often diffuse, which makes its exact delimitation complicated. We can see how the proposed network delimits this contour in a similar way to the experts, without significant differences. In Figure 6 it can be seen how this network obtains accurate segmentation results in images obtained from both peripapillary and macula regions. This network is able to adapt to different types of images, where the texture and shape of the choroid changes very abruptly, producing robust segmentation of this layer under highly variable conditions. This approach is followed by UNet using Efficientnet-b7 as the encoder. From the results, it can be seen how, in general, FPN seems to perform better using a Densenet type encoder, while UNet seems to perform better using an Efficientnet type encoder. The Densenet type encoder, through its dense connections, seems to contribute in a better way to make the set of final FPN multiscale feature maps more coherent with each other. For the UNet case, the Efficientnet encoder seems to better extract the features of each scale individually improving the reconstruction of the final feature maps. Models using Efficientnet-b0 as the encoder obtain the worst segmentation results. As can be seen in Figure 4, these models produce false positives in regions that do not belong to the choroid. This encoder is much smaller so it has a smaller number of parameters (4M) than the Densenet201 (18M) or the Efficientnet-b7 (63M). A smaller encoder can, a priori, help to generalize better and reduce possible overfitting in small datasets like ours. However, in this problem, it does not work since the size of the model limits its ability to accommodate the intense variety of textures and shapes presented by the choroid in the image set.

4. Conclusions

Many routine clinical studies as well as longitudinal studies collected in the past have been created without using the EDI protocol or similar variants. In addition, the use of OCT images obtained in a single region of the eye (either macular or peripapillary) and with a specific parameter setting is limited in their potential clinical utility. In this paper, we present several approaches to accurately segment the choroid in OCT non-EDI images with varying configurations. We demonstrate how several architectures, most notably the FPN with a Densenet201 encoder, is capable of robustly accomplishing this task. This network outperforms the state of the art and is able to segment the choroid in images with different texture and shape characteristics. We showed its effectiveness on several datasets and prove that the lower boundary of the choroid predicted by the network does not differ significantly from those labeled manually by different clinical experts. This segmentation is performed accurately and automatically in both healthy subjects and MS patients which facilitates the use of choroid appearance as a biomarker. This helps the clinical expert in the task of diagnosis and follow-up of this disease, lightening his work and reducing the subjectivity of the process. In the future, this method can be integrated into a larger system that uses the complete 3D OCT cubes to make a comprehensive analysis of the patient.

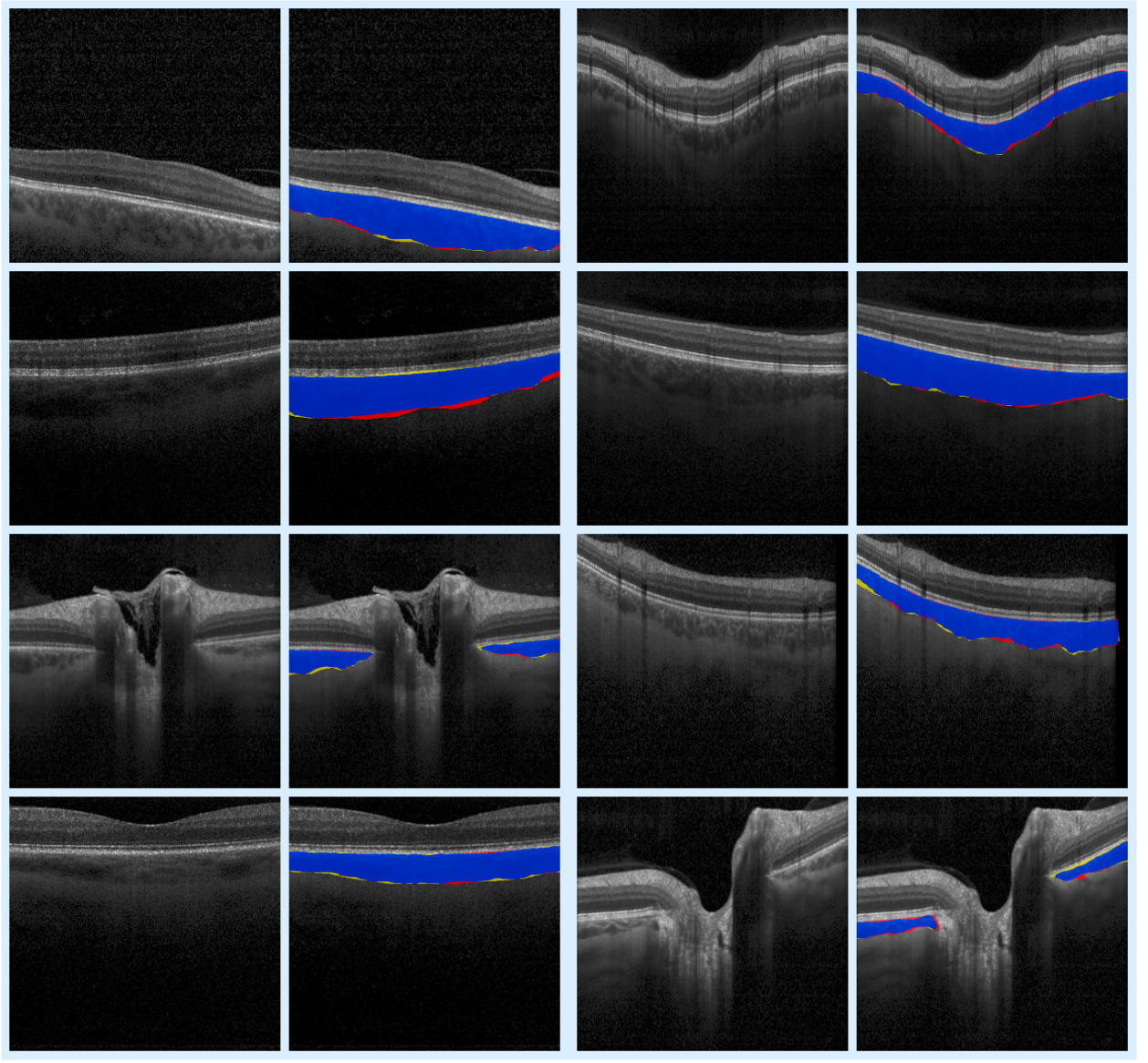

Fig. 6. Multiple examples of the segmentation masks predicted by the FPN model with Densenet201 encoder. The predicted areas that match the labeling are shown in blue while the false positives and false negatives are shown in red and yellow, respectively.

Acknowledgements

This research was funded by Instituto de Salud Carlos III, Government of Spain, DTS18/00136 research project; Ministerio de Ciencia e Innovación y Universidades, Government of Spain, RTI2018-095894-B-I00 research project; Ministerio de Ciencia e Innovación, Government of Spain through the research project with reference PID2019-108435RB-I00; Consellería de Cultura, Educación e Universidade, Xunta de Galicia, Grupos de Referencia Competitiva, grant ref. ED431C 2020/24; Axencia Galega de Innovación (GAIN), Xunta de Galicia, grant ref. IN845D 2020/38; CITIC, Centro de Investigación de Galicia ref. ED431G 2019/01, receives financial support from Consellería de Educación, Universidade e Formación Profesional, Xunta de Galicia, through the ERDF (80%) and Secretaría Xeral de Universidades (20%). Emilio López Varela acknowledges its support under FPI Grant Program through PID2019-108435RB-I00 project.

References

[1] Borkovkina, S., Camino, A., Janpongsri, W., Sarunic, M.V., Jian, Y., 2020. Real-time retinal layer segmentation of oct volumes with gpu accelerated inferencing using a compressed, low-latency neural network. Biomedical optics express 11, 3968–3984.

[2] Britze, J., Frederiksen, J.L., 2018. Optical coherence tomography in multiple sclerosis. Eye 32, 884–888.

[3] Chen, M., Wang, J., Oguz, I., VanderBeek, B.L., Gee, J.C., 2017. Automated segmentation of the choroid in edi-oct images with retinal pathology using convolution neural networks, in: Fetal, Infant and Ophthalmic Medical Image Analysis. Springer, pp. 177–184.

[4] Deng, J., Dong, W., Socher, R., Li, L.J., Li, K., Fei-Fei, L., 2009. Imagenet: A large-scale hierarchical image database, in: 2009 IEEE conference on computer vision and pattern recognition, Ieee. pp. 248–255.

[5] Di Staso, F., Ciancaglini, M., Abdolrahimzadeh, S., D'APOLITO, F., Scuderi, G., 2019. Optical coherence tomography of choroid in common neurological diseases. in vivo 33, 1403–1409.

[6] Doğan, Ü., Ulaş, F., Türkoğlu, Ş.A., Ögün, M.N., Ağca, S., 2019. Eyes are mirror of the brain: comparison of multiple sclerosis patients and healthy controls using oct. International Journal of Neuroscience 129, 848–855.

[7] Esen, E., Sizmaz, S., Demir, T., Demirkiran, M., Unal, I., Demircan, N., 2016. Evaluation of choroidal vascular changes in patients with multiple sclerosis using enhanced depth imaging optical coherence tomography. Ophthalmologica 235, 65–71.

[8] Garcia-Martin, E., Jarauta, L., Vilades, E., Ara, J.R., Martin, J., Polo, V., Larrosa, J.M., Pablo, L.E., Satue, M., 2018. Ability of swept-source optical coherence tomography to detect retinal and choroidal changes in patients with multiple sclerosis. Journal of ophthalmology 2018.

[9] George, N., Jiji, C., 2019. Two stage contour evolution for automatic segmentation of choroid and cornea in oct images. Biocybernetics and biomedical Engineering 39, 686–696.

[10] Hagens, M.H., Burggraaff, J., Kilsdonk, I.D., de Vos, M.L., Cawley, N., Sbardella, E., Andelova, M., Amann, M., Lieb, J.M., Pantano, P., et al., 2018. Three-tesla mri does not improve the diagnosis of multiple sclerosis: a multicenter study. Neurology 91, e249–e257.

[11] Huang, G., Liu, Z., Van Der Maaten, L., Weinberger, K.Q., 2017. Densely connected convolutional networks, in: Proceedings of the IEEE conference on computer vision and pattern recognition, pp. 4700–4708.

[12] Kajić, V., Esmaeelpour, M., Považay, B., Marshall, D., Rosin, P.L., Drexler, W., 2012. Automated choroidal segmentation of 1060 nm oct in healthy and pathologic eyes using a statistical model. Biomedical optics express 3, 86–103.

[13] Li, J., Jin, P., Zhu, J., Zou, H., Xu, X., Tang, M., Zhou, M., Gan, Y., He, J., Ling, Y., et al., 2021. Multi-scale gcn-assisted two-stage network for joint segmentation of retinal layers and discs in peripapillary oct images. Biomedical Optics Express 12, 2204–2220.

[14] Lin, T.Y., Dollár, P., Girshick, R., He, K., Hariharan, B., Belongie, S., 2017. Feature pyramid networks for object detection, in: Proceedings of the IEEE conference on computer vision and pattern recognition, pp. 2117–2125.

[15] Long, J., Shelhamer, E., Darrell, T., 2015. Fully convolutional networks for semantic segmentation, in: Proceedings of the IEEE conference on computer vision and pattern recognition, pp. 3431–3440.

[16] López-Varela, E., Vidal, P.L., Pascual, N.O., Novo, J., Ortega, M., 2022. Fully-automatic 3d intuitive visualization of age-related macular degeneration fluid accumulations in oct cubes. Journal of Digital Imaging , 1–12.

[17] Medeiros, F.A., Zangwill, L.M., Bowd, C., Vessani, R.M., Susanna Jr, R., Weinreb, R.N., 2005. Evaluation of retinal nerve fiber layer, optic nerve head, and macular thickness measurements for glaucoma detection using optical coherence tomography. American journal of ophthalmology 139, 44–55.

[18] Merino, A.G., Callizo, J.A., Fernández, O.F., Pascual, L.L., Torres, E.M., Zarrantz, A.R.A., 2017. Consenso para el tratamiento de la esclerosis múltiple 2016. sociedad española de neurología. Neurología 32, 113–119.

[19] Moeskops, P., Viergever, M.A., Mendrik, A.M., De Vries, L.S., Benders, M.J., Išgum, I., 2016. Automatic segmentation of mr brain images with a convolutional neural network. IEEE transactions on medical imaging 35, 1252–1261.

[20] Paszke, A., Gross, S., Massa, F., Lerer, A., Bradbury, J., Chanan, G., Killeen, T., Lin, Z., Gimelshein, N., Antiga, L., et al., 2019. Pytorch: An imperative style, high-performance deep learning library. Advances in neural information processing systems 32.

[21] Ronneberger, O., Fischer, P., Brox, T., 2015. U-net: Convolutional networks for biomedical image segmentation, in: International Conference on Medical image computing and computer-assisted intervention, Springer. pp. 234–241.

[22] Salafian, B., Kafieh, R., Rashno, A., Pourazizi, M., Sadri, S., 2018. Automatic segmentation of choroid layer in edi oct images using graph theory in neutrosophic space. arXiv preprint arXiv:1812.01989 .

[23] Sicras-Mainar, A., Ruíz-Beato, E., Navarro-Artieda, R., Maurino, J., 2017. Impact on healthcare resource utilization of multiple sclerosis in spain. BMC Health Services Research 17, 1–7.

[24] Spaide, R.F., Koizumi, H., Pozonni, M.C., 2008. Enhanced depth imaging spectral-domain optical coherence tomography. American journal of ophthalmology 146, 496–500.

[25] Tan, M., Le, Q., 2019. Efficientnet: Rethinking model scaling for convolutional neural networks, in: International conference on machine learning, PMLR. pp. 6105–6114.

[26] Wallin, M.T., Culpepper, W.J., Campbell, J.D., Nelson, L.M., Langer-Gould, A., Marrie, R.A., Cutter, G.R., Kaye, W.E., Wagner, L., Tremlett, H., et al., 2019. The prevalence of ms in the united states: a population-based estimate using health claims data. Neurology 92, e1029–e1040.

[27] Wang, J., Zhang, M., Pechauer, A.D., Liu, L., Hwang, T.S., Wilson, D.J., Li, D., Jia, Y., 2016. Automated volumetric segmentation of retinal fluid on optical coherence tomography. Biomedical optics express 7, 1577–1589.

[28] Wang, R.K., 2002. Signal degradation by multiple scattering in optical coherence tomography of dense tissue: a monte carlo study towards optical clearing of biotissues. Physics in Medicine & Biology 47, 2281.

[29] Xie, H., Pan, Z., Zhou, L., Zaman, F.A., Chen, D.Z., Jonas, J.B., Xu, W., Wang, Y.X., Wu, X., 2022. Globally optimal oct surface segmentation using a constrained ipm optimization. Optics Express 30, 2453–2471.

[30] Yakubovskiy, P., 2020. Segmentation models pytorch. https://github.com/qubvel/segmentation_models.pytorch.